Chapter 14
Nanoscale Investigation of Porous Structure in Adsorption-Desorption Cycles in the MgO-Al_2O_3 Ceramics

H. Klym, A. Ingram, R. Szatanik, and I. Hadzaman

14.1 Introduction

It is known that among a large number of porous materials used for humidity sensors [1–6], spinel ceramics is one of the best. Functional ceramics, in particular MgO-Al_2O_3 ceramics, are thermally and chemically more stable compared with other types of porous materials with a short reaction time to change humidity [7–9]. In addition, the materials of active elements of humidity sensors based on ceramics do not require additional processes after technological optimization.

As noted in [10–15], the functionality of ceramic materials is determined by the microstructure of their grains, intergranular boundaries, and pores of different sizes and shapes. These elements, in general, depend on the characteristics of sintering ceramics and significantly affect its nanostructure [16–19]. In addition, the operational electrical properties of humidity-sensitive elements depend on the sorption processes, the surface area, and the sufficient amount of nanopore in the material [20–22]. Therefore, it is important to study the processes of nanostructured materials with developed porosity and optimal pore size distribution [19, 23, 24]. It is the void inclusion in ceramic materials that significantly affects their exploitation properties [19, 25].

H. Klym (✉)
Lviv Polytechnic National University, Lviv, Ukraine
e-mail: halyna.i.klym@lpnu.ua

A. Ingram · R. Szatanik
Opole University of Technology, Opole, Poland

I. Hadzaman
Drohobych State Pedagogical University, Drohobych, Ukraine

O. Fesenko, L. Yatsenko (eds.), *Nanocomposites, Nanostructures, and Their Applications*, Springer Proceedings in Physics 221,
https://doi.org/10.1007/978-3-030-17759-1_14

Traditionally, microstructural features of materials are studied using X-ray diffraction, electron microscopy, porosimetric equipment, etc. [26–28]. However, methods for Hg and N_2 porosimetry are limited in use, since it provides information about open nanoscale pores with radius of >5 nm and >2 nm, respectively. It is known that physical processes in ceramics depend not only on the amount and nature of large open pores but also on nanoporous and free-volume vacancies, vacancy clusters, defects, etc. [29]. Therefore, in order to obtain more information about these structural inhomogeneities and their influence on the properties of ceramics MgO-Al_2O_3, it is also helpful to use additional structural research methods that allow studying pores and volumetric inclusion at the nanoscale level. In this case, positron annihilation lifetime (PAL) method is one of the most powerful experimental methods for studying internal structural voids in solids [30–32].

Previously, in studying the structural features of the MgO-Al_2O_3 ceramic by the PAL method, it was shown that two processes can take place in this material: the positron trapping in defects (two components) and ortho-positronium (*o-Ps*) decaying (one component) obtained in the expansion of three components [20–23, 33]. Within the framework of this approach, the short-term component of the PAL spectrum with the lifetime τ_1 reflects the microstructural features of the spinel, the mean component with lifetime τ_2—defects near the intergranular boundaries. The third component with lifetime τ_3 is related to the "pick-off" annihilation of *o-Ps* in intergranular nanoporous filled with adsorbed water [20–22, 33, 34]. Using the lifetime of the third component, it was possible to calculate the radii of nanopores according to the Tao-Eldrup model [35–37]. However, for such a material as humidity-sensitive ceramics MgO-Al_2O_3, there are nanopores of different sizes and different natures [17, 23, 24, 38], the study of which by PAL method requires its modification and optimization.

The aim of this work is nanoscale investigation of pores in adsorption-desorption cycles in the MgO-Al_2O_3 ceramics sintered at 1400 °C for 2 hours using the modified PAL method at four-component spectrum decomposition procedure.

14.2 Experimental Details

The PAL study was performed using the ORTEC spectrometer (full width at half the maximum was 0.27 ns, a separation of 230 ps) at a temperature of 22 °C and an initial relative humidity of 35% [39–41]. Two identical test specimens were placed on both sides of the positron source (^{22}Na isotope, activity ~ 50 kBq) from an aqueous solution of ^{22}NaCl wrapped in a special Kapton® foil with a thickness of 12 μm.

The scheme of the experimental setup for obtaining lifetime spectra is depicted in Fig. 14.1. The signal of an initial 1.27 MeV γ-quantum recorded by the γ-scintillator is converted into an analog electrical pulse in a photomultiplier connected to this scintillator. The signal emitted from the anode of this photomultiplier and gets

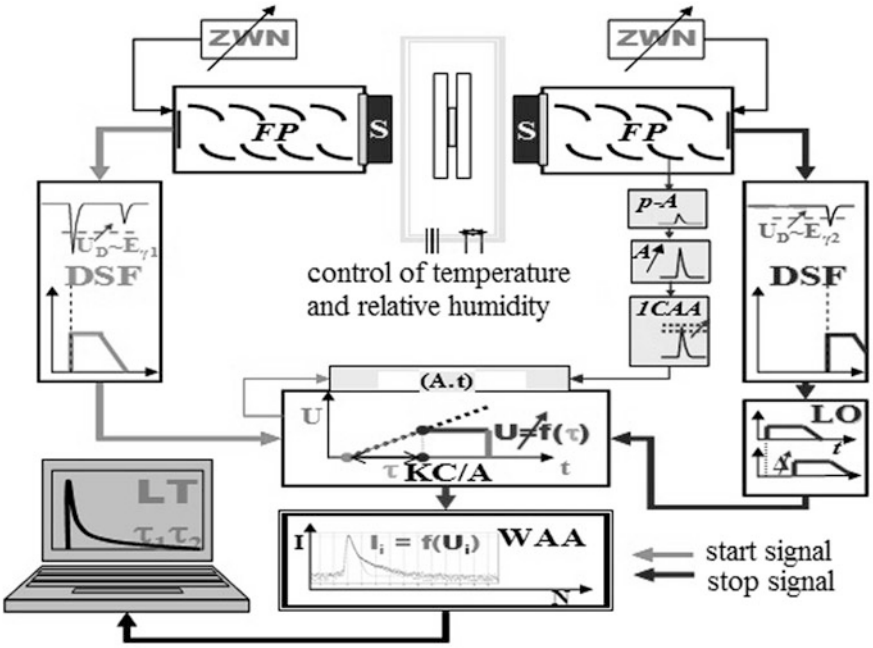

Fig. 14.1 Measuring PAL system based on ORTEC spectrometer [42]

through a constant discriminator serves as the initial signal for the time pulse converter [42].

The second scintillator registers one of two γ-quanta with an energy of 0.511 MeV. The corresponding signal from the photomultiplier anode is compared in a time pulse converter with a signal from the dynode of this photomultiplier, previously processed by the amplifier of the signal, an amplifier, and a one-channel analyzer. When changing the electrical parameters of the delay line, the initial zero-time position of the measured spectrum is selected.

The amplitude of the output signal obtained from the converter is proportional to the difference between the occurrence of the initial and final γ-quanta or the residence time of the positron. Analog-digital signal is recorded in the memory of the multichannel analyzer; the data is fed to a personal computer. Thus, a complete spectrum of the lifetime of a positron is obtained (the dependence of the number of channels or the number of counts from the positron lifetimes).

For statistical surveys with a high number of measurements, investigation was made using the PAL-modified hardware complexity with a modernized digital analog converter KC/A and a multichannel (8000 channels) WAA amplitude analyzer. This is possible to simultaneously register two annihilation spectra: up to 50 ns with a resolution of 6.15 ps and up to 500 ns with a resolution of 61.5 ps [42, 43]. The modified circuit for measuring the PAL spectra is shown in Fig. 14.2.

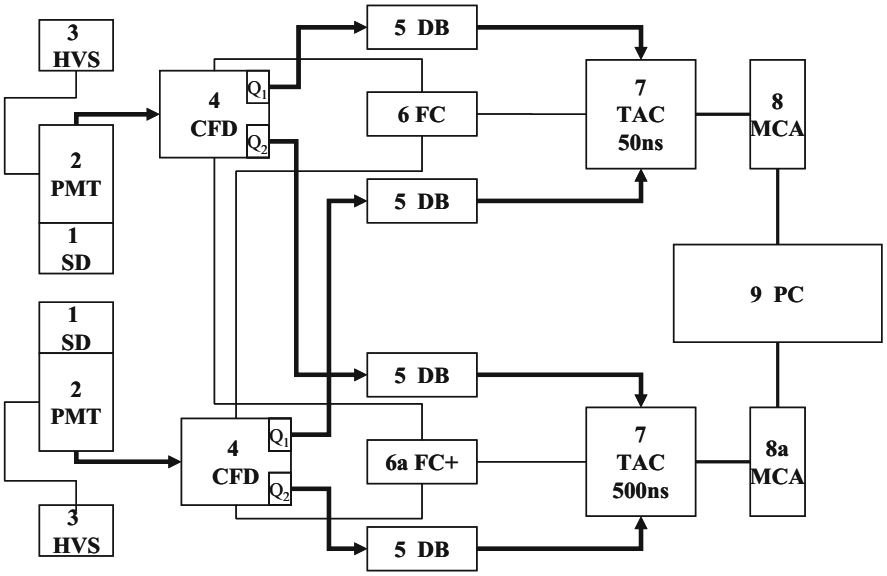

Fig. 14.2 Modified PAL system using ORTEC [43]

Such studies make it possible to obtain information in the expansion of the spectrum into three and four components for a material with advanced nanoporosity (humidity-sensitive $MgO\text{-}Al_2O_3$ ceramics). For the pairs of samples, three measurements of the PAL spectrum were used, which differed in the total number of simple annihilation events [24]. Each spectrum was repeatedly processed due to minor changes in the number of final channels, the background of annihilation, and the time of change in the spectrum. The best results were selected on the basis of the fit, defined as the lowest mean deviation between the experimental points and the theoretical curve [42]:

$$\mathrm{FIT} = \frac{\sum_{k=1}^{N}\left(\frac{T_k - E_k}{\sqrt{E_k}}\right)^2}{N-m} \approx \frac{1}{N}\sum_{k=1}^{N}\left(\frac{T_k - E_k}{\sqrt{E_k}}\right)^2, \tag{14.1}$$

where N is the number of channels (or number of experimental points), E_k experimentally measured number of counts in the kth channel, T_k theoretical number of counts in kth channel, $\sqrt{E_k}$ mean square deviation of the number of counts in the kth channel, m number of fitting parameters.

Thus, in the final result several groups with different numbers of experimental points N were formed in the middle of the chosen procedure of mathematical fitting. Only results with FIT values close to 1 (from 0.95 to 1.1–1.2) were considered to be absolutely relevant. In the next step, these values and the specific characteristics of the PAL were monitored, depending on the annihilation background and the time of

change in the spectrum. It should be noted that the correction for the source and the spectrometer solution function remained constant for the entire spectrum [23, 24, 44].

By working out the PAL spectra by the LT program [45–48], it is possible to obtain the values of the fitting parameters (lifetimes and intensities). Positron trapping parameters in ceramic MgO-Al_2O_3, such as bulk lifetime τ_b, average lifetime τ_{av}, and the rate of positron trapping in defects κ_d, were calculated in accordance with the two-state positron trapping modes [49–51]. The difference $(\tau_2 - \tau_b)$ was evaluated as the size of bulk defects, which occupy positrons.

14.3 Results and Discussion

Since MgO-Al_2O_3 ceramics are humidity-sensitive materials, the main structural component is open nanoscale pores. Using the modified PAL method and performing additional adsorption-desorption procedures [20–22, 42], the processes in nanopores of this material can be studied. So, PAL experiments were carried out in the MgO-Al_2O_3 ceramics sintered at 1400 °C using high-statistical measurements.

Initial measurements were performed in ceramics dried in a vacuum at 120 °C for 4 hours. To study the interconnection of porous structure of ceramics, the same specimens were immersed in water (placed in the distiller, relative humidity was 100%) for 8 hours (1 day) at a temperature of 22 °C. Measurement of the PAL spectra was repeated 7 days after this procedure. At the last stage, samples of ceramics were again dried in vacuum at 120 °C for 4 hours, and measurements by the PAL method were repeated to determine the reversibility of the physical sorption of water molecules [24, 33, 44].

For the maximum estimation of free volume in ceramic samples and calculation of the nanopore size, the PAL spectra were decomposed by the LT program into four components with lifetimes τ_1, τ_2, τ_3, and τ_4, as well as intensities I_1, I_2, I_3, and I_4 [24, 44]. The third and fourth components of the spectrum reflect the annihilation of *o-Ps* through the "pick-off" process, including water-immersed nanopores. The PAL spectrum treatment using four-component treatment due to the application of modified measurement method, which allows to expand the research area, is depicted in Fig. 14.3.

The *o-Ps* lifetime ($\tau_{o\text{-}Ps}$) in ceramic materials (the lifetime of the third and fourth components of PAL spectrum) can be related with average radius of nanopores (R) and calculated by the semiempirical Tao-Eldrup model [36, 37]:

$$\tau_{o-Ps} = \left[2\left(1 - \frac{R}{R+\Delta R} + \frac{1}{2\pi}\sin\left(\frac{2\pi R}{R+\Delta R}\right)\right) + 0.007\right]^{-1}, \qquad (14.2)$$

where ΔR is an empirically determined parameter (in the classical case $\Delta R \approx 0.1656$ nm) which describes the effective thickness of electronic layer responsible for "pick-off" annihilation of *o-Ps* in voids.

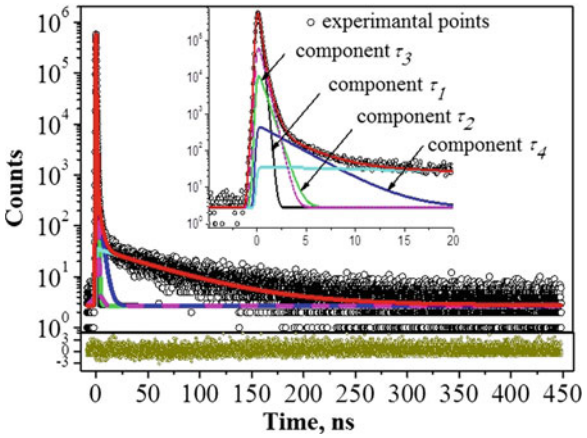

Fig. 14.3 PAL spectra for the MgO-Al_2O_3 ceramics decomposed into four components [42]

Table 14.1 PAL parameters and size of free volumes in the MgO-Al_2O_3 ceramics sintered at 1400 °C in adsorption-desorption cycles: initial ceramics (1), after immersion (2), final dried (3)

	Fitting parameters							
Prehistory	τ_1, ns	I_1, a.u.	τ_2, ns	I_2, a.u.	τ_3, ns	I_3, a.u.	τ_4, ns	I_4, a.u.
1	0.152	0.88	0.388	0.11	2.504	0.007	62.32	0.008
2	0.160	0.77	0.409	0.20	2.562	0.022	57.35	0.006
3	0.154	0.89	0.402	0.10	2.539	0.007	61.85	0.008
Prehistory	Positron trapping modes							
	$\tau_{av.}$, ns		τ_b, ns		κ_d, ns^{-1}		$\tau_2 - \tau_b$, ns	
1	0.178		0.16		0.44		0.23	
2	0.211		0.18		0.78		0.23	
3	0.179		0.16		0.40		0.24	

In addition to the radii of nanopores (R_3 and R_4) calculated from the Tao-Eldrup model, the contribution of the corresponding nanopores by semiempirical relation is determined as [42]:

$$f_v = C \cdot V_f \cdot I_{o-Ps}, \tag{14.3}$$

where $V_f = 4/3 \cdot \pi \cdot R_{o-Ps}$ is free volume calculated using the lifetime of the *o-Ps*-related components in spherical approximation, $I_{o\text{-}Ps}$ is the intensity of the *o-Ps*-related components, and C is an empirical parameter equal to 0.0018.

As can be seen from Table 14.1, after water immersion of the MgO-Al_2O_3 ceramics, the lifetime of the second component τ_2 and the intensity of I_2 increase, which shows the intensification of positron trapping in defects near intergranular boundaries [20–22]. After drying, the intensity values are virtually returned to their initial values, while the lifetime exceeds the initial value. Thus, adsorption processes of water in the MgO-Al_2O_3 ceramics are accompanied by fragmentation of voids and desorption—their agglomeration. The change in the positron capture parameters

correlates with changes in the parameters of the first and second components of PAL spectra.

At water immersion of ceramics, the lifetime of the fourth component τ_4 is accompanied by a decrease in the intensity I_4, while a decrease of lifetime τ_3 leads to an increase in the intensity I_3. In the first case, the decrease of the lifetime τ_4 and the intensity I_4 is due to the arrangement of the layer of water molecules along the walls of the nanopores, which is accompanied by a decrease in the size of the free volume, where the *o-Ps* atoms are captured. In the second case, the *o-Ps* annihilation mechanism is more complicated. The decay of *o-Ps* atoms can occur both in dry nanopores and in the bubbles of water by the "pick-off" process. The last process leads to an increase in the intensity I_3. The contribution of the nanopore with size R_4 is much higher than the pore with radius R_3 (Fig. 14.4). Consequently, the modified multichannel positron annihilation model in the MgO-Al_2O_3 ceramics [44] besides the positron trapping channel contains a decay channel of *o-Ps* atoms, which reflects two different annihilation processes in two types of nanopores: "pick-off" annihilation *o-Ps* in water adsorbed by small nanopores due to "bubble" mechanism and in a free volume of larger nanopores filled by water [52].

Thus, PAL method gives information about nanoscale pores in addition to Hg-porosimetry data [23] (Fig. 14.5).

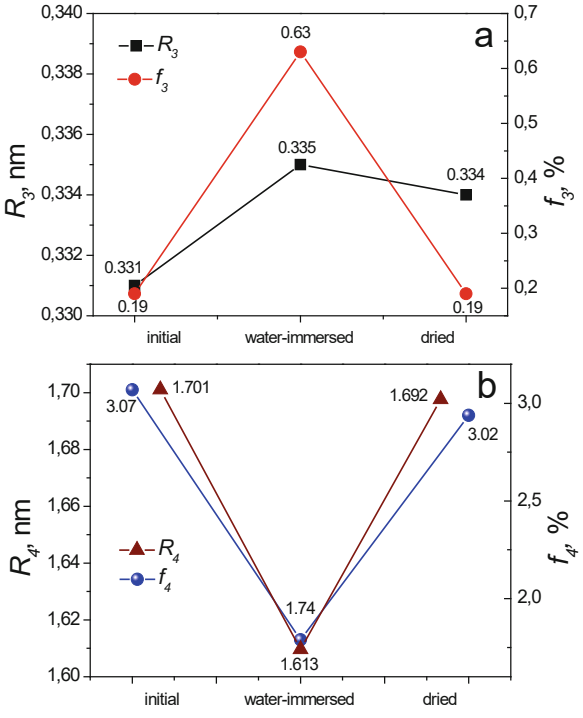

Fig. 14.4 Dependences of the radii of nanopores R_3 and R_4 (**a**) and fraction f_3 and f_4 (**b**) on the conditions of watering and drying

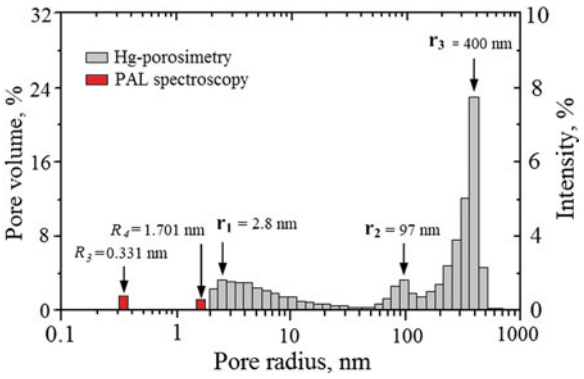

Fig. 14.5 Pore size distributions of MgO-Al_2O_3 ceramics sintered at 1400 °C: Hg-porosimetry [23] and PAL data (for initial ceramics)

In addition, water also affects the parameters of positron trapping in defects near intergranular boundaries (the second component of the PAL spectrum). Changes in the parameters of the second and third components under the influence of water are the same. With regard to the use of the fourth component, two different approaches can be applied. Within the framework of the first one, it is possible to estimate the influence of physically and chemically adsorbed water [22] on the modification of intergranular boundaries in ceramics during immersion. In accordance with the second approach, one can study the patterns of nanostructured MgO-Al_2O_3 ceramics under influence of absorbed water by all nanoporous of ceramics. The second and third components of the PAL spectra are interconnected; for ceramics positronium positrons (the second component) can replace traps (the third component). The fourth component reflects completely different processes in larger nanopores during their immersion. Therefore, in the first approach, we can assume that this component does not affect the positron trapping in defects near intergranular boundaries.

14.4 Conclusions

It is shown that using PAL method for the investigation of nanoscale pores in the MgO-Al_2O_3 ceramic, it is possible to obtain information on size of nanopores of ceramics (according to Tao-Eldrup model) and to study the processes occurring in these ceramics. The spectrum schedule for the four components also allowed modifying the multichannel positron trapping model, which combines two channels: positron trapping channel and decay of the *o-Ps* atoms. The third component describes "pick-off" process of *o-Ps* annihilation in small nanopores and in water, and the fourth component is related to annihilation of *o-Ps* in the volume of larger nanopores not filled by water.

Acknowledgments H. Klym thanks Ministry of Education and Science of Ukraine for support. The authors thank Prof. O. Shpotyuk for discussion.

References

1. Kulwicki BM (1991) Humidity sensors. J Am Ceram Soc 74(4):697–708. https://doi.org/10.1111/j.1151-2916.1991.tb06911.x
2. Chen Z, Lu C (2005) Humidity sensors: a review of materials and mechanisms. Sens Lett 3(4):274–295. https://doi.org/10.1166/sl.2005.045
3. Bearzotti A, Bertolo JM, Innocenzi P, Falcaro P, Traversa E (2004) Humidity sensors based on mesoporous silica thin films synthesised by block copolymers. J Eur Ceram Soc 24(6):1969–1972. https://doi.org/10.1016/S0955-2219(03)00521-1
4. Hadzaman I, Klym H, Shpotuyk O, Brunner M (2010) Temperature sensitive spinel-type ceramics in thick-film multilayer performance for environment sensors. Acta Physica Polonica-Series A 117(1):234–237. http://przyrbwn.icm.edu.pl/APP/PDF/117/a117z148.pdf
5. Rittersma ZM, Splinter A, Bödecker A, Benecke W (2000) A novel surface-micromachined capacitive porous silicon humidity sensor. Sens Actuators B Chem 68(1–3):210–217. https://doi.org/10.1016/S0925-4005(00)00431-7
6. Farahani H, Wagiran R, Hamidon MN (2014) Humidity sensors principle, mechanism, and fabrication technologies: a comprehensive review. Sensors 14(5):7881–7939. https://doi.org/10.3390/s140507881
7. Gusmano G, Montesperelli G, Traversa E (1993) Microstructure and electrical properties of $MgAl_2O_4$ thin film for humidity sensors. J Am Ceram Soc 76:743–750. https://doi.org/10.1111/j.1151-2916.1993.tb03669.x
8. Traversa E (1995) Ceramic sensors for humidity detection: the state-of-the-art and future developments. Sensors Actuators 23:135–156. https://doi.org/10.1016/0925-4005(94)01268-M
9. Gusmano G, Montesperelli G, Nunziante P, Traversa E (1993) Study of the conduction mechanism of $MgAl_2O_4$ at different environmental humidities. Electrochim Acta 38(17):2617–2621. https://doi.org/10.1016/0013-4686(93)80160-2
10. Gleiter H (2000) Nanostructured materials: basic concepts and microstructure. Acta Mater 48(1):1–29. https://doi.org/10.1016/S1359-6454(99)00285-2
11. Li Y, Fu ZY, Su BL (2012) Hierarchically structured porous materials for energy conversion and storage. Adv Funct Mater 22(22):4634–4667. https://doi.org/10.1002/adfm.201200591
12. Dillon SJ, Harmer MP (2007) Multiple grain boundary transitions in ceramics: a case study of alumina. Acta Mater 55(15):5247–5254. https://doi.org/10.1016/j.actamat.2007.04.051
13. Weaver PM, Cain MG, Stewart M, Anson A, Franks J, Lipscomb IP, McBride JP, Zheng D, Swingler J (2012) The effects of porosity, electrode and barrier materials on the conductivity of piezoelectric ceramics in high humidity and dc electric field smart materials and structures. Smart Mater Struct 21(4):045012. https://doi.org/10.1088/0964-1726/21/4/045012
14. Armatas GS, Salmas CE, Louloudi MG, Androutsopoulos P, Pomonis PJ (2003) Relationships among pore size, connectivity, dimensionality of capillary condensation, and pore structure tortuosity of functionalized mesoporous silica. Langmuir 19:3128–3136. https://doi.org/10.1021/la020261h
15. Kashi MA, Ramazani A, Abbasian H, Khayyatian A (2012) Capacitive humidity sensors based on large diameter porous alumina prepared by high current anodization. Sensors Actuators A 174:69–74. https://doi.org/10.1016/j.sna.2011.11.033
16. Vakiv M, Hadzaman I, Klym H, Shpotyuk O, Brunner M (2011) Multifunctional thick-film structures based on spinel ceramics for environment sensors. J Phys Conf Ser 289(1):012011. https://doi.org/10.1088/1742-6596/289/1/012011
17. Klym H, Hadzaman I, Shpotyuk O, Ingram A (2018) Grain porous structure and exploitation properties of humidity-sensitive magnesium aluminate spinel-type ceramics. Springer Proc Phys 214:499–519. https://doi.org/10.1007/978-3-319-92567-7_32

18. Wang W, Fu Z, Wang H, Yuan R (2002) Influence of hot pressing sintering temperature and time on microstructure and mechanical properties of TiB2 ceramics. J Eur Ceram Soc 22(7):1045–1049. https://doi.org/10.1016/S0955-2219(01)00424-1
19. Klym H, Hadzaman I, Shpotyuk O (2015) Influence of sintering temperature on pore structure and electrical properties of technologically modified MgO-Al_2O_3 ceramics. Mater Sci 21(1):92–95. https://doi.org/10.5755/j01.ms.21.1.5189
20. Filipecki J, Ingram A, Klym H, Shpotyuk O, Vakiv M (2007) Water-sensitive positron-trapping modes in nanoporous magnesium aluminate ceramics. J Phys Conf Ser 79(1):012015. https://doi.org/10.1088/1742-6596/79/1/012015
21. Klym H, Ingram A, Shpotyuk O, Hadzaman I, Solntsev V (2016) Water-vapor sorption processes in nanoporous MgO-Al_2O_3 ceramics: the PAL spectroscopy study. Nanoscale Res Lett 11(1):1. https://doi.org/10.1186/s11671-016-1352-6
22. Klym H, Ingram A, Shpotyuk O, Hadzaman I, Chalyy D (2018) Water-sorption effects near grain boundaries in modified MgO-Al_2O_3 ceramics tested with positron-positronium trapping algorithm. Acta Phys Pol A 133(4):864–868. https://doi.org/10.12693/APhysPolA.133.864
23. Klym H, Ingram A, Hadzaman I, Shpotyuk O (2014) Evolution of porous structure and free-volume entities in magnesium aluminate spinel ceramics. Ceram Int 40(6):8561–8567. https://doi.org/10.1016/j.ceramint.2014.01.070
24. Klym H, Ingram A, Shpotyuk O, Hadzaman I, Hotra O, Kostiv Y (2016) Nanostructural free-volume effects in humidity-sensitive MgO-Al_2O_3 ceramics for sensor applications. J Mater Eng Perform 25(3):866–873. https://doi.org/10.1007/s11665-016-1931-9
25. Sommers A, Wang Q, Han X, T'Joen C, Park Y, Jacobi A (2010) Ceramics and ceramic matrix composites for heat exchangers in advanced thermal systems – a review. Appl Therm Eng 30(11-12):1277–1291. https://doi.org/10.1016/j.applthermaleng.2010.02.018
26. Asami K, Mitani S, Fujimori H, Ohnuma S, Masumoto T (1999) Characterization of Co-Al-O magnetic thin films by combined use of XPS, XRD and EPMA. Surf Interface Anal 28:250–253. https://doi.org/10.1002/(SICI)1096-9918(199908)28:1<250::AID-SIA587>3.0.CO;2-T
27. Asami K, Ohnuma T (1998) Masumoto XPS and X-ray diffraction characterization of thin Co-Al-N alloy films prepared by reactive sputtering deposition. Surf Interface Anal 26:659–666. https://doi.org/10.1002/(SICI)1096-9918(199808)26:9<659::AID-SIA412>3.0.CO;2-Z
28. Moreira EA, Coury JR (2004) The influence of structural parameters on the permeability of ceramic foams. Braz J Chem Eng 21(1):23–33. https://doi.org/10.1590/S0104-66322004000100004
29. Ferraris E, Vleugels J, Guo Y, Bourell D, Kruth JP, Lauwers B (2016) Shaping of engineering ceramics by electro, chemical and physical processes. CIRP Ann 65(2):761–784. https://doi.org/10.1016/j.cirp.2016.06.001
30. Chakraverty S, Mitra S, Mandal K, Nambissan PMG, Chattopadhyay S (2005) Positron annihilation studies of some anomalous features of $NiFe_2O_4$ nanocrystals grown in SiO_2. Phys Rev B 71(2):024115. https://doi.org/10.1103/PhysRevB.71.024115
31. Tuomisto F, Makkonen I (2013) Defect identification in semiconductors with positron annihilation: experiment and theory. Rev Mod Phys 85(4):1583. https://doi.org/10.1103/RevModPhys.85.1583
32. Krause-Rehberg R, Leipner HS (1999) Positron annihilation in semiconductors. Defect studies. Springer, Berlin/Heidelberg/New York, p 378
33. Klym H, Ingram A, Shpotyuk O, Hadzaman I (2012) Water-sorption processes in nanostructured ceramics for sensor electronics studied with positron annihilation instruments. 28th international conference on microelectronics (MIEL), p 155–158. https://doi.org/10.1109/MIEL.2012.6222821
34. Klym H, Ingram A, Shpotyuk O, Filipecki J (2010) PALS as characterization tool in application to humidity-sensitive electroceramics. 27th international conference on microelectronics proceedings (MIEL), p 239–242. https://doi.org/10.1109/MIEL.2010.5490492
35. Goworek T (2002) Comments on the relation: positronium lifetime–free volume size parameters of the Tao–Eldrup model. Chem Phys Lett 366(1-2):184–187. https://doi.org/10.1016/S0009-2614(02)01569-5

36. Tao SJ (1972) Positronium annihilation in molecular substance. J Chem Phys 56(11):5499–5510. https://doi.org/10.1063/1.1677067
37. Eldrup M, Lightbody D, Sherwood JN (1981) The temperature dependence of positron lifetimes in solid pivalic acid. Chem Phys 63:51–58. https://doi.org/10.1016/0301-0104(81)80307-2
38. Klym H, Vasylchyshyn I, Hadzaman I, Dunets R (2018) Porous structure and exploitation properties of nanostructured MgO-Al_2O_3 ceramics technologically modified by time-temperature regimes. 38th international conference on Electronics and Nanotechnology (ELNANO), p 142–145. https://doi.org/10.1109/ELNANO.2018.8477514
39. Shpotyuk O, Calvez L, Petracovschi E, Klym H, Ingram A, Demchenko P (2014) Thermally-induced crystallization behaviour of 80$GeSe_2$-20Ga_2Se_3 glass as probed by combined X-ray diffraction and PAL spectroscopy. J Alloys Compd 582:323–327. https://doi.org/10.1016/j.jallcom.2013.07.127
40. Klym H, Ingram A, Shpotyuk O, Calvez L, Petracovschi E, Kulyk B, Serkiz R, Szatanik R (2015) 'Cold' crystallization in nanostructurized 80$GeSe_2$-20Ga_2Se_3 glass. Nanoscale Res Lett 10(1):1–8. https://doi.org/10.1186/s11671-015-0775-9
41. Klym H, Ingram A, Shpotyuk O, Hadzaman I, Solntsev V, Hotra O, Popov AI (2016) Positron annihilation characterization of free volume in micro-and macro-modified $Cu_{0.4}Co_{0.4}Ni_{0.4}Mn_{1.8}O_4$ ceramics. Low Temp Phys 42(7):601–605. https://doi.org/10.1063/1.4959021
42. Klym H, Shpotyuk O, Ingram A, Karbovnyk I (2018) Modified positron annihilation lifetime spectroscopy method for investigation of nanomaterials with advanced porosity. 38th international conference on Electronics and Nanotechnology (ELNANO), p 134–137. https://doi.org/10.1109/ELNANO.2018.8477443
43. Klym HI, Ivanusa AI, Kostiv YM, Chalyy DO, Tkachuk TI, Dunets RB, Vasylchyshyn II (2017) Methodology and algorithm of multicomponent analysis of positron annihilation spectra for nanostructured functional materials. J Nano-Electron Phys 9(3):03037-1–03037-6. https://doi.org/10.21272/jnep.9(3).03037
44. Klym H, Karbovnyk I, Vasylchyshyn I (2016) Multicomponent positronium lifetime modes to nanoporous study of MgO-Al_2O_3 ceramics. 13th international conference on modern problems of radio engineering, Telecommunications and Computer Science (TCSET), p 406–408. https://doi.org/10.1109/TCSET.2016.7452071
45. Giebel D, Kansy J (2011) A new version of LT program for positron lifetime spectra analysis. Mater Sci Forum 666:138–141. https://doi.org/10.4028/www.scientific.net/MSF.666.138
46. Kansy J (2001) Programs for positron lifetime analysis adjusted to the PC windows environment. Mater Sci Forum 363:652–654
47. Kansy J, Consolati G, Dauwe C (2000) Positronium trapping in free volume of polymers. Radiat Phys Chem 58(5-6):427–431. https://doi.org/10.1016/S0969-806X(00)00195-X
48. Kansy J (2000) Positronium trapping in free volume of polymers. Radiat Phys Chem 58:427–431. https://doi.org/10.1016/S0969-806X(00)00195-X
49. Kansy J (1996) Microcomputer program for analysis of positron annihilation lifetime spectra. Nucl Instrum Methods Phys Res, Sect A 374(2):235–244. https://doi.org/10.1016/0168-9002(96)00075-7
50. Ghosh S, Nambissan PMG, Bhattacharya R (2004) Positron annihilation and Mössbauer spectroscopic studies of In^{3+} substitution effects in bulk and nanocrystaline $MgMn_{0.1}Fe_{1.9-x}O_4$. Phys Lett A 325:301–308. https://doi.org/10.1016/j.physleta.2004.03.062. Get rights and content
51. Nambissan PMG, Upadhyay C, Verma HC (2003) Positron lifetime spectroscopic studies of nanocrystalline $ZnFe_2O_4$. J Appl Phys 93:6320. https://doi.org/10.1063/1.1569973
52. Guo Z, Liang X, Pereira T, Scaffaro R, Hahn HT (2007) CuO nanoparticle filled vinyl-ester resin nanocomposites: fabrication, characterization and property analysis. Compos Sci Technol 67(10):2036–2044. https://doi.org/10.1016/j.compscitech.2006.11.017